This is an open access article published under an ACS AuthorChoice License, which permits copying and redistribution of the article or any adaptations for non-commercial purposes.

ACS OMEGA

Article

Cite This: ACS Omega 2018, 3, 15510−15518

http://pubs.acs.org/journal/acsodf

Pyrene Bearing Azo-Functionalized Porous Nanofibers for CO_2 Separation and Toxic Metal Cation Sensing

Oussama M. El-Kadri,*[,†,‡] Tsemre-Dingel Tessema,[§] Ruaa M. Almotawa,[∥] Ravi K. Arvapally,[∥] Mohammad H. Al-Sayah,[†,‡] Mohammad A. Omary,[∥,⊥] and Hani M. El-Kaderi*[,§]

[†]Department of Biology, Chemistry, and Environmental Sciences, and [‡]Materials Science and Engineering Research Institute, American University of Sharjah, P.O. Box 26666, Sharjah, United Arab Emirates

[§]Department of Chemistry, Virginia Commonwealth University, 1001 W. Main Street, Richmond, Virginia 23284-2006, United States

[∥]Department of Chemistry and Advanced Materials and Manufacturing Processes Institute (AMMPI), University of North Texas, 1155 Union Circle #305070, Denton, Texas 76203, United States

[⊥]Institute of New Energy, Science Hall, 1003 Shangbu Road, Shenzhen 518031, China

Supporting Information

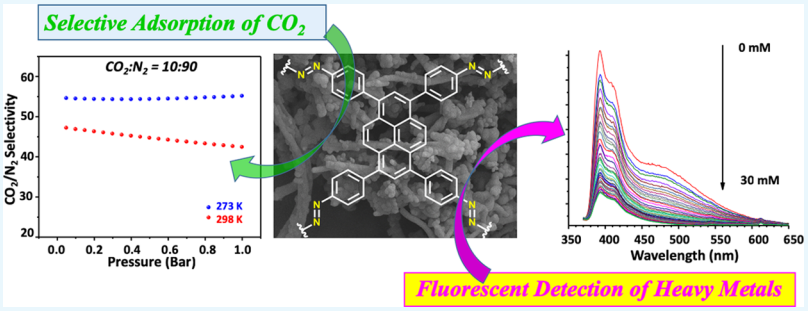

ABSTRACT: A novel luminescent azo-linked polymer (ALP) has been constructed from 1,3,6,8-tetra(4-aminophenyl)pyrene using a copper(I)-catalyzed oxidative homocoupling reaction. The polymer displays high porosity with a Brunauer−Emmett−Teller surface area of 1259 $m^2\ g^{-1}$ and narrow pore size distribution (1.06 nm) and is able to take up a significant amount of CO_2 (2.89 mmol g^{-1}) at 298 K and 1.00 bar with a high isosteric heat of adsorption of 27.5 kJ mol^{-1}. Selectivity studies applying the ideal adsorbed solution theory revealed that the novel polymer has moderately good selectivities for CO_2/N_2 (55.1) and CO_2/CH_4 (10.9). Furthermore, the ALP shows fluorescence quenching in the presence of Hg^{2+}, Pb^{2+}, Tl^{+}, and Al^{3+} ions. Compared with these ions, the ALP showed no sensitivity to light metal ions such as Na^{+}, K^{+}, and Ca^{2+} in ethanol−water solution, clearly indicating the high selectivity of the ALP toward heavy metal ions. The exceptional physiochemical stability, high porosity, and strong luminescence make this polymer an excellent candidate as a fluorescent chemical sensor for the detection of heavy metal ions.

1. INTRODUCTION

Porous organic polymers (POPs) are an emerging class of materials that have witnessed increasing interest because of their applications in gas storage and separation,[1−4] catalysis,[5−10] sensing,[11−15] and optoelectronics.[16,17] Such diverse applications stem from the numerous available building blocks and various synthetic routes that allow the design and construction of different POPs tailored for specific applications. Because of their exceptional physiochemical stability, high surface area, and structure/function tunability, POPs have been widely explored for the capture and separation of carbon dioxide (CO_2), a gas that is linked directly to climate change and global warming.[1−4,18,19] It is well documented that POPs containing polar chemical functionalities and Lewis basic sites show enhanced CO_2 binding energy, presumably via hydrogen bonding, dipole−quadrupole interactions, and Lewis acid−base interactions, thus leading to an improvement in CO_2 uptake and selectivity over gases such as nitrogen and methane.[20−22] Introduction of polar functional groups such as amines into the POP frameworks such as amine, which provide CO_2-philic sites, has been explored using both post- and presynthetic modification of sorbents.[23−27] However, such synthetic routes, in general, suffer from the use of expensive transition metal-based catalysts, multistep reactions, and extensive purification steps and hence are not practical for large-scale preparation. In addition, amine-decorated POPs show limited chemical stability because of their proneness to oxidative degradation in air, whereas imine-linked POPs suffer

Received: August 6, 2018
Accepted: October 26, 2018
Published: November 14, 2018

© 2018 American Chemical Society

DOI: 10.1021/acsomega.8b01920
ACS Omega 2018, 3, 15510−15518

from poor CO_2/N_2 selectivity, especially at elevated temperatures.[27] To avoid such drawbacks, others and we have recently reported a low-cost and efficient synthetic route for the preparation of a series of azo-linked polymers (ALPs).[2,28−30] The nitrogen−nitrogen double bonds (azo-bonds) in such porous materials provide the Lewis basic sites that are needed for the CO_2 molecules to interact with the framework without compromising the chemical stability as the case in amine-based POPs. Not surprisingly, these ALPs showed remarkable physiochemical stability, high CO_2 uptake capacities, and good CO_2/N_2 selectivity at ambient conditions.[2,29]

Besides CO_2 capture, the detection of heavy metal ions also poses another environmental and health challenge addressed in this work. Natural resource pollution is a huge problem especially water contaminated with heavy metals such as mercury, lead, and thallium, which are extremely toxic to the environment as well for human consumption.[31] A recent example of such contamination of drinking water by the lead metal from industrial sources was reported in Flint, Michigan in 2015.[32] The incident had a devastating effect on public health, where many people have reported lead-poisoning symptoms and a huge economic cost. Such incidents impose a challenging problem to the scientific community to develop fast-response sensor systems for continuous monitoring of drinking water sources and for remediation of contaminations. Luminescent sensors represent potential solutions for sensitive and selective detection of heavy metal contaminants of drinking water; a recent example has shown detection limits as low as parts per billion levels for Ag^+ ions and parts per million levels for lead and thallium by a phosphorescent molecular/polymeric composite chemosensor.[33]

The synergistic functionalities and properties of POPs containing rich π-conjugated building blocks decorated with heteroatoms, and high surface areas provide docking sites and broad interface for metals' interaction, which allow enhancement in the signaling sensitivity.[13,15,34,35] In addition, the recyclability of POP sensors can be easily achieved because of the weak interaction (physisorption) of the analytes and the frameworks of POPs. Another added advantage of POPs as sensors is the plentiful apertures' availability, leading to increase in the diffusion rates and thereby faster response times. Despite such attractive properties that POPs offer, their use as chemical sensors is not well-developed and mostly limited to the detection of nitroaromatic compounds.[36−38]

With the above considerations and challenges in mind, herein, we report on the synthesis and characterization of a new azo-bond-functionalized polymer bearing a pyrene moiety, Azo-Py. The novel azo-linked porous polymer was synthesized using a 1,3,6,8-tetra(4-aminophenyl)pyrene monomer and a CuBr-catalyzed oxidative homocoupling reaction.[39] We have shown that the electron-rich and rigid pyrene core of 1,3,6,8-tetra(4-aminophenyl)pyrene leads to a highly porous polymer and exhibits a solid-state packing behavior, resulting in a nanofiber morphology.[21] This was facilitated by $\pi-\pi$ stacking of the highly conjugated pyrene group. The CO_2 uptake and selectivity of Azo-Py were studied for flue gas and landfill gas mixtures. Furthermore, because of its excellent fluorescence properties, the potential utility of Azo-Py as a selective chemosensor for the detection of heavy metal ions (such as mercury, lead, and thallium, among others) was also investigated.

2. EXPERIMENTAL SECTION

2.1. General Techniques and Materials. All solvents, starting materials, and reagents were purchased from Acros Organics and used without any further purification unless otherwise noted. 4-Aminophenylboronic acid pinacol ester and tetrakis(triphenylphosphine)palladium(0) were purchased from Aldrich. Air-sensitive materials and reactions were handled or carried out in an inert atmosphere (nitrogen gas) using a glovebox or Schlenk line techniques. 1,3,6,8-Tetra(4-aminophenyl)pyrene was prepared according to literature procedures.[40] Elemental analysis was performed for carbon, nitrogen, and hydrogen on an Euro EA3000 Series CHN elemental analyzer (EuroVector Instruments). ^{1}H NMR was conducted using a Varian Mercury-400 MHz NMR spectrometer. Fourier-transform infrared (FTIR) spectra were obtained using a Nicolet Nexus 670 spectrometer equipped with an attenuated total reflectance accessory. The thermal stability of the synthesized polymers was assessed using a Perkin thermo-gravimetric analyzer with a temperature ramp rate of 5 °C/min under N_2 flow. Scanning electron microscopy (SEM) images were obtained to the morphology of the polymers using a Hitachi SU-70 FE-SEM. The samples were prepared by dispersion onto a double-sided carbon tape attached to the sample holder, followed by a platinum coating for 70 s at 1×10^{-6} bar. Powder X-ray diffraction data were collected using a PANalytical X'Pert PRO multipurpose diffractometer by Cu Kα radiation with a 2θ range of 2−30.

2.2. Gas Uptake Studies. Porosity and gas uptake studies were conducted using a Quantachrome Autosorb iQ volumetric analyzer using gases of ultrahigh-purity grade. Typically, an Azo-Py sample (∼40−50 mg) was loaded into a preweighed 9 mm large bulb Quantachrome cell, which was then hooked up to the degassing station of the gas analyzer. The sample was then degassed at 120 °C and 1.0×10^{-5} bar for 12 h. The degassed sample and cell were refilled with helium, weighed, and hooked up to the analysis station of the gas analyzer. Adsorption temperatures were attained using a temperature-controlled water/ethylene glycol mixture bath for 273 and 298 K and a refrigerated bath of liquid nitrogen for 77 K.

2.3. Photoluminescence Studies. The photoluminescence measurements were obtained with a PTI QuantaMaster model QM-4 scanning spectrofluorometer. The instrument has the capabilities to measure near-infrared (IR) luminescence with the attached accessory along with the direct quantum yield using a spherical integration sphere, which is attached to the sample chamber. A suspension of the polymer (0.1 mg/1 mL) in the corresponding solvent was sonicated for 15 min at room temperature and was then placed (3 mL) in a quartz cuvette. Aliquots of the metal solutions (0.1 M) were added, and the fluorescence spectrum (λ_{exc} = 360 nm) was recorded after every addition. Mercury salt ($HgBr_2$) was dissolved in acetonitrile, whereas the metal solution ($NaNO_3$, KNO_3, $Ca(NO_3)_2$, $Pb(NO_3)_2$, $TlNO_3$, and $AlCl_3$) was prepared in methanol/water (2:3) solutions. **Caution**: Thallium compounds are highly toxic in nature and extra caution (e.g., wearing triple gloves) is to be taken while handling them.

2.4. Synthesis of Azo-Py. Azo-Py was synthesized following a procedure established and further optimized by El-Kaderi et al.[2,30] A solution of CuBr (25 mg, 0.174 mmol) and pyridine (110 mg, 1.391 mmol) in 11 mL of toluene was stirred at 25 °C for 3 h in a 50 mL round-bottom flask and an

DOI: 10.1021/acsomega.8b01920
ACS Omega 2018, 3, 15510−15518

open air atmosphere. To this solution, 1,3,6,8-tetra(4-aminophenyl)pyrene (100 mg, 0.176 mmol) dissolved in 11 mL tetrahydrofuran (THF) was added. The mixture was stirred in an open air atmosphere at 25 °C for 24 h and refluxed at 60 °C for 12 h and then at 80 °C for 12 h. A burgundy colored solid was isolated by filtration and subsequently washed with THF and water. The obtained powder was stirred in HCl (100 mL, 2 M) for 12 h, filtered, and then washed with water. The powder was further treated with NaOH (2 M), water, ethanol, THF, and chloroform. The final product was dried at 120 °C under vacuum (150 mTorr) to give Azo-Py as a burgundy colored powder (82 mg, 83%). Anal. Calcd for $C_{40}H_{22}N_4$: C, 86.00%; H, 3.97%; N, 10.03%. Found: C, 70.76%; H, 4.39%; N 8.23%.

3. RESULTS AND DISCUSSION

3.1. Synthesis and Characterization of Azo-Py. Azo-Py was prepared via an oxidative homocoupling of aniline-functionalized monomer with a pyrene core, yielding robust azo-bonded linkages as presented in Scheme 1.

Scheme 1. Synthetic Route for the Preparation of Azo-Py

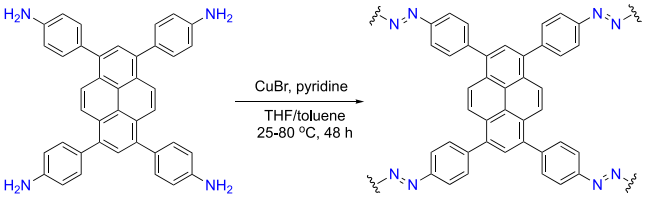

This polymerization reaction was carried out following our recent report, which outlined the optimum molar amount of CuBr, solvent composition, and temperature ramp profile in order to enhance the porosity of the resulting polymer.[2] Azo-Py is insoluble in common organic solvents such as water, THF, chloroform, toluene, and ethanol—depicting its structure as a highly cross-linked framework. Polymerization of Azo-Py was confirmed using Fourier transform IR (FTIR) spectroscopy (Figure S1). Vibrational bands in the region of 1415−1400 cm^{-1} signify the presence of azo bonds expected in Azo-Py. Also, the decrease in intensity of the N−H stretching bands at 3200−3450 cm^{-1} indicates the consumption of secondary amine groups of the monomers taking part in the azo-bond formation. It should be noted that unreacted terminal amines are seen as expected in the FTIR spectra of Azo-Py. SEM imaging (Figure 1A) shows that Azo-Py formed a nanofibrous morphology similar to previously reported benzimidazole-linked polymers (BILPs) bearing a pyrene core.[21,41] It is presumed that these nanofibers, which are about 0.2 μm in thickness and of varying length, result from $\pi-\pi$ stacking interactions induced by the rigid and highly-conjugated pyrene core. The thermal stability of Azo-Py was assessed by thermogravimetric analysis (TGA), which showed stability up to near 500 °C (Figure 1B). Powder X-ray diffraction revealed an amorphous material as there were no distinct peaks in the spectra (Figure S2).

3.2. Porosity and Textural Properties. The porosity and textural properties of Azo-Py were characterized from its nitrogen isotherm at 77 K (Figure 1C). A steeply-increasing uptake is observed at lower pressure ranges (P/P_o < 0.035), followed by a decline in the slope of uptake in higher pressure ranges (P/P_o ∼ 0.035−0.9). This trend is indicative of a highly microporous material with a minor mesoporous pore size distribution (PSD).[42,43] The textural properties of Azo-Py are summarized in Table 1. The 1259 m^2 g^{-1} Brunauer−Emmett−

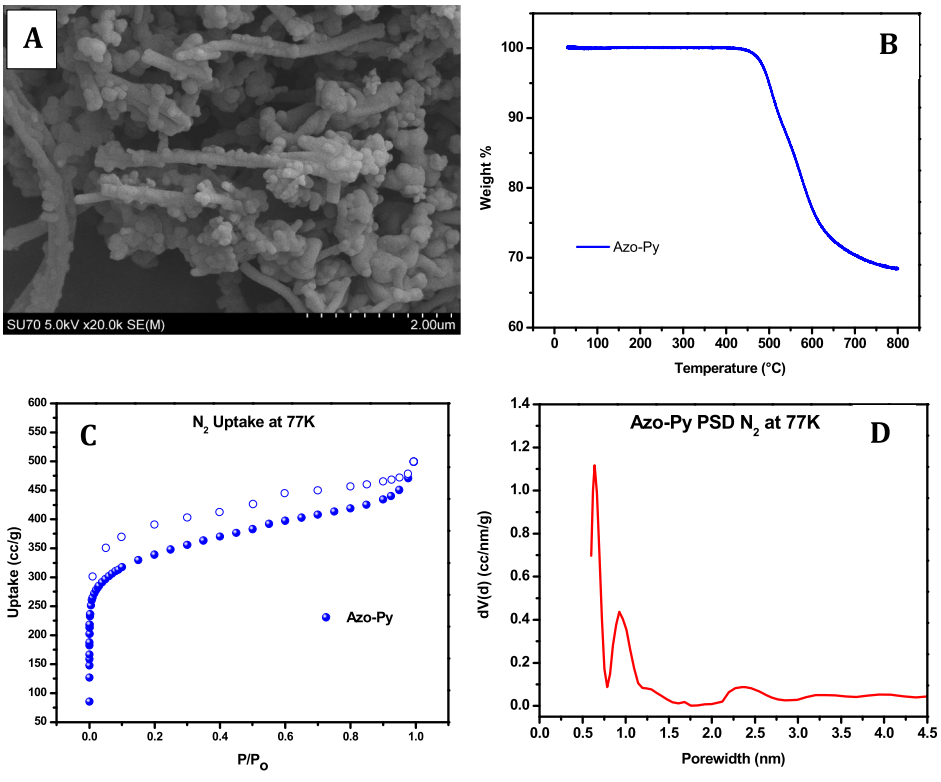

Figure 1. (A) SEM, (B) TGA, (C) N_2 sorption−desorption isotherm at 77 K, and (D) PSD of Azo-Py.

DOI: 10.1021/acsomega.8b01920
ACS Omega 2018, 3, 15510−15518

Table 1. Textural Properties of Azo-Py

	[a]$SA_{(BET)}$ (m^2 g^{-1})	[b]PSD (nm)	[c]pore vol. (cm^{-3} g^{-1})	[d]$vol._{(Mic)}$ (cm^{-3} g^{-1})	[e]$vol._{(U. Mic)}$ (cm^{-3} g^{-1})
Azo-Py	1259	1.06	0.699	0.377	0.0158

[a]BET surface area. [b]Dominant pore size determined by QSDFT fittings of N_2 isotherms at 77 K. [c]Total pore volume at P/P_o = 0.95. [d]Micropore volume determined by DFT (the values in parenthesis are the percentage of micropore volume relative to the total pore volume). [e]Pore volume of ultra-micropores (< 0.7 nm) determined from CO_2 isotherms at 273 K.

Teller (BET) surface area of Azo-Py is higher than previously reported azo-bond-functionalized POPs including ALPs (412−1235 m^2 g^{-1}),[2,30] azo-COPs (493−729 m^2 g^{-1}),[20] and azo-POFs (439−712 m^2 g^{-1}).[44] Particularly, the surface area is higher than that in some of the BILPs bearing a pyrene backbone including BILP-10, 11, and 13 (658−787 m^2 g^{-1}).[21] A direct comparison can be made with BILP-10 (787 m^2 g^{-1}) as it is the benzimidazole-linked analogue to Azo-Py. In this case, the superior surface area of Azo-Py is a testament to the optimized synthetic route implemented for achieving high porosity in ALPs that we recently reported.[2] However, BILP-12 displays a higher surface area than Azo-Py because of the incorporated triptycene building which has an internal molecular free volume (IMFV).[45] A PSD curve was generated by fitting the adsorption branch of the N_2 isotherm at 77 K to quenched solid density functional theory (QSDFT) model for slit and cylindrical pores for carbon (Figure 1D). The curve shows a dominant pore size centered at 0.64 nm for Azo-Py. The total pore volume of the polymer was deduced from a single adsorption point, at P/P_o = 0.95, and found to be 0.699 cm^3 g^{-1}. The micropore volume was also determined to be 0.377 cm^3 g^{-1} making up 53.9% of the total pore volume. Additionally, the profile of ultra-micropores (< 0.7 nm) was elucidated by nonlocalized DFT fitting of the adsorption branch of the CO_2 isotherm at 273 K (Figure S3) with the ultra-micropore volume quantified to be 0.016 cm^3 g^{-1}.

3.3. Gas Uptake and Selectivity Studies. The textural properties discussed above, including the high surface area, microporous nature, and narrow pore size have proven to be effective in enhancing the CO_2 uptake in porous frameworks. Additionally, the incorporation of azo-bonds in porous sorbents has been theoretically and experimentally validated to enhance CO_2 uptake facilitated via Lewis acid−base interactions between CO_2 and the azo functionalities.[22] With that in consideration, the gas uptake capacity of Azo-Py was investigated by collecting low-pressure CO_2, CH_4, and N_2 isotherms at 273 and 298 K presented in Figure 2 and summarized in Table 2. The CO_2 isotherms display a steep rise in the low-pressure region and no hysteresis in the adsorption and desorption curves characteristic of sorbents that can be regenerated at a low energy penalty. At 273 K and 1 bar, Azo-Py has a CO_2 uptake of 4.79 mmol g^{-1}, which is higher than BILP-10, -11, and -13 (2.6−4.0 mmol g^{-1}). Consistent with the surface area difference, Azo-Py had a lower CO_2 uptake than BILP-12 (5.1 mmol g^{-1}).[41] This is indicative of the direct correlation between the surface area and CO_2 uptake that has been observed in most porous polymers. In relation to other azo-functionalized polymers, Azo-Py has a higher CO_2 uptake at 273 K and 1 bar than all ALPs (2.5−4.7 mmol g^{-1}) except for ALP-1 (5.37 mmol g^{-1}).[2,30] While at 298 K and 1 bar, Azo-Py has a CO_2 uptake of 2.89 mmol g^{-1} which is higher than azo-COPs (1.2−1.5 mmol g^{-1}) and azo-POFs (1.2−1.5 mmol g^{-1}) but slightly lower than ALP-1 (3.2 mmol g^{-1}) and ALP-5 (2.94 mmol g^{-1}). This is due to the triptycene-based framework of ALP-1 which results in high IMFV, enhancing the total uptake at 1 bar, while ALP-5 has a high binding affinity to CO_2 because of its narrow pore size. The CH_4 uptake of Azo-Py at 1 bar was recorded at 1.54 and 0.89 mmol g^{-1} at 273 and 298 K, respectively. This was higher than all pyrene-derived BILPs[41] and all ALPs except ALP-1. The binding affinity of Azo-Py for gas molecules was quantified via isosteric heat of adsorption, Q_{st}, by fitting the CO_2 and CH_4 isotherms at 273 and 298 K, respectively, with the virial equation. The CO_2 Q_{st} value for Azo-Py at zero surface coverage was quantified to be 27.5 kJ mol^{-1}. From the Q_{st} curves generated (Figure 3), it is evident that the strength of interaction between gas molecules and the polymer pore walls decreases with more loading as the interaction sites and pore volumes are increasingly saturated. The Q_{st} for CH_4 was calculated to be 22.6 kJ mol^{-1} with depreciation in binding affinity observed with increasing gas loading as well.

Motivated by the azo-functionality, microporous nature, high CO_2 uptake, and suitable binding affinity of Azo-Py, the

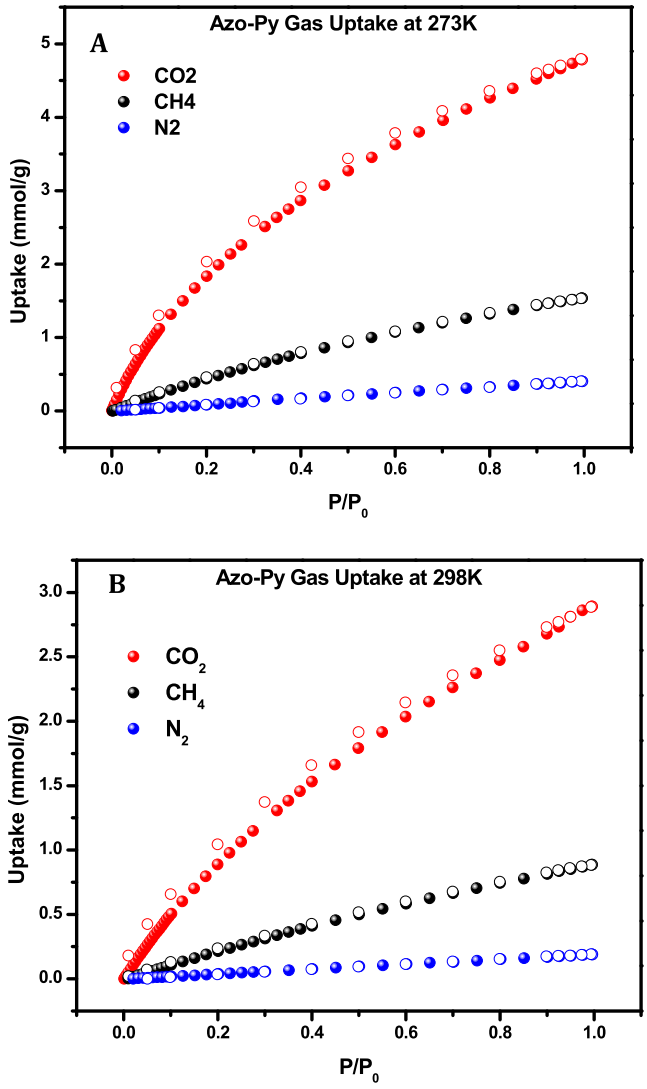

Figure 2. CO_2, CH_4, and N_2 uptake isotherms of Azo-Py at 273 K (A) and 298 (B). Open and closed circle symbols denote adsorption and desorption, respectively.

DOI: 10.1021/acsomega.8b01920
ACS Omega 2018, 3, 15510−15518

Table 2. Gas Uptakes, Heat of Adsorption, and Selectivity of Azo-Py[a]

	CO_2 uptake at 1 bar			CH_4 uptake at 1 bar			N_2 uptake at 1 bar		selectivity	
adsorbent	273 K	298 K	Q_{st}	273 K	298 K	Q_{st}	273 K	298 K	CO_2/N_2	CO_2/CH_4
Azo-Py	4.79	2.89	27.5	1.54	0.89	22.6	0.40	0.19	55.1 (42.4)	10.9 (7.8)

[a]Gas uptake in mmol g^{-1}, and isosteric heat of adsorption (Q_{st}) at zero coverage in kJ mol^{-1}. Selectivity (mol mol^{-1}, at 1.0 bar) calculated by the IAST method at the mole ratio of 10:90 for CO_2/N_2 and the mole ratio of 50:50 for CO_2/CH_4 at 273 and 298 K.

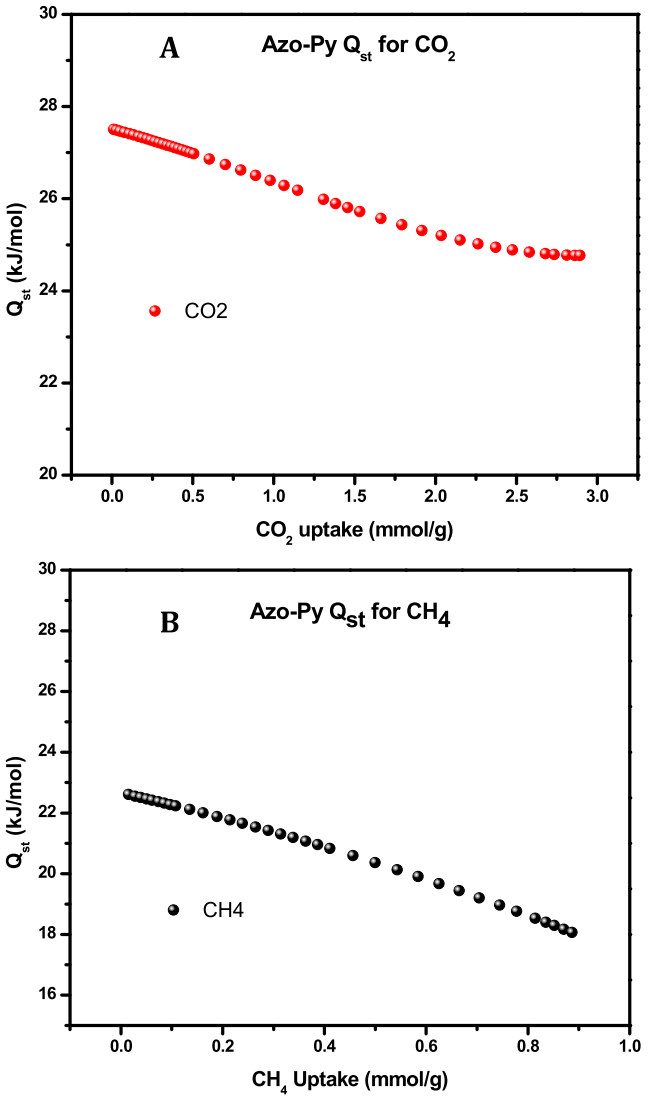

Figure 3. Azo-Py isosteric heat of adsorption for CO_2 (A) and CH_4 (B).

selective CO_2 capture potential of Azo-Py was evaluated from the analysis of single gas isotherms of CO_2, CH_4, and N_2 using two methods: Henry's law constants and the ideal adsorbed solution theory (IAST). Henry's law constants were obtained from the initial slope of the adsorption branch of the isotherms (Figure S5a–d). The CO_2/N_2 selectivities were found to be 39.6 (273 K) and 29.2 (298 K), whereas CO_2/CH_4 selectivities were 7.04 (273 K) and 4.8 (298 K). IAST is a widely recognized method for deducing the selective gas capture behavior of porous sorbents from single gas isotherms while considering the composition of the targeted gas mixtures at adsorption conditions. In this case, flue gas composed predominantly of CO_2 and N_2 with ratios of CO_2/N_2 at 10:90 and landfill gas composed predominantly of CO_2 and CH_4 with ratios of CO_2/CH_4 at 50:50 were analyzed (Figure 4). For flue gas compositions, the CO_2/N_2 IAST selectivity of

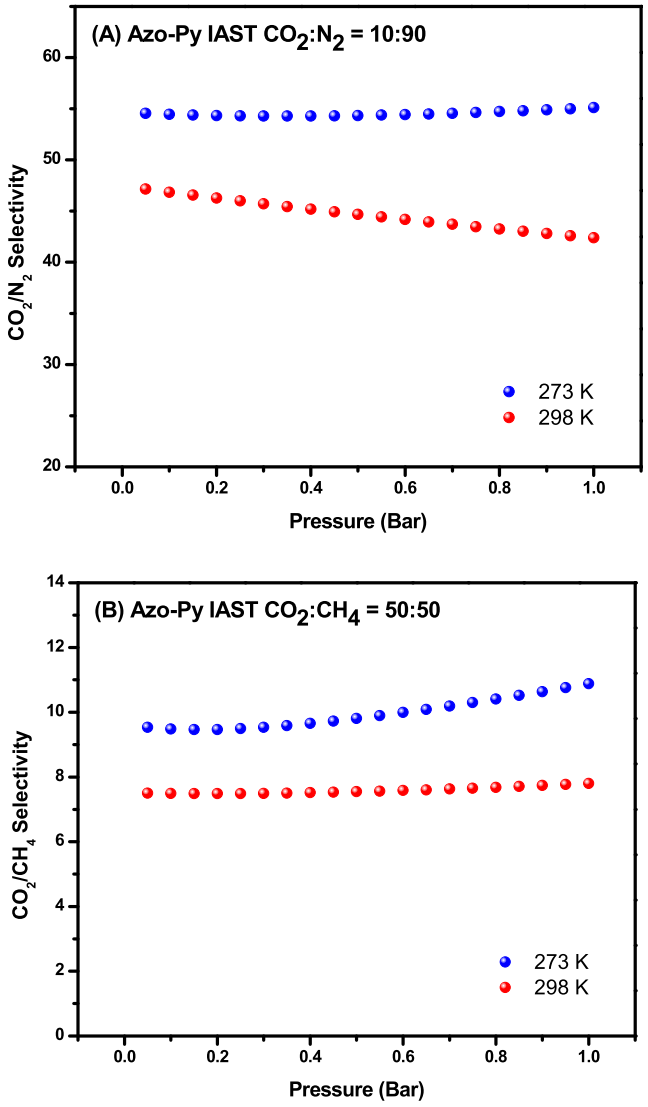

Figure 4. IAST selectivity of CO_2/N_2 (10:90) (A) and CO_2/CH_4 (50:50) (B) at 273 and 298 K, respectively.

Azo-Py at 1 bar was calculated at 55.1 and 42.4 at 273 and 298 K, respectively. These values are comparable to other nitrogen-bearing organic polymers ALPs,[2,30] BILPs,[46] and functionalized NPOFs.[24] The decrease in selectivity from 273 to 298 K is a trend that has been observed before in POPs that lack the presence of a large portion of pores in the mesoporous range.[47,48] The CO_2/CH_4 selectivity of Azo-Py at 1 bar was 10.9 and 7.8 for 273 and 298 K, respectively. These values are also comparable to our previously published azo-functionalized polymers.

DOI: 10.1021/acsomega.8b01920
ACS Omega 2018, 3, 15510–15518

3.4. Photoluminescence and Metal-Sensing Studies.

The structural architecture of Azo-Py consists of a two-dimensional -network of pyrene-based backbone linked through the azo-group moieties. This provides a π-electron-rich conjugated system with strong emission intensities, similar to that of pyrene. Figure 5 shows the fluorescence profile of

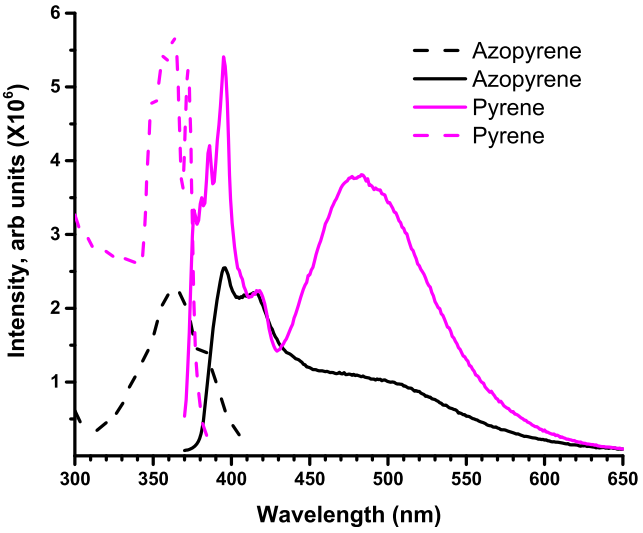

Figure 5. Excitation (dotted lines) and the emission (solid lines) spectra for pyrene (λ_{exc} = 360 nm and λ_{emi} = 395 nm) and Azo-Py (λ_{exc} = 360 nm and λ_{emi} = 415 nm), respectively.

Azo-Py, which is similar to that of pure pyrene in acetonitrile. Azo-Py exhibits mainly a monomer emission peak at ~415 nm with a less significant excimer emission at ~490 nm.[36,49] Perturbations of the electronic distribution of the π-electrons in this conjugated system through the electrostatic interaction of metal ions would change the emission profile of the polymer;[50,51] hence, the azopyrene polymers can be utilized as a fluorescent chemical sensor for metal ions.

To test the efficacy of Azo-Py as a sensor for metal ions, we investigated the effect of the presence of sodium, potassium, calcium, mercury, lead, thallium, and aluminum ions on the emission of the polymer in solution. Millimolar concentrations of each metal's salt solution were titrated into a uniform suspension of the azopyrene polymer in acetonitrile (0.1 mg/mL), and the fluorescence spectrum of the polymer was monitored after every addition. Figure 6 shows the change in the fluorescence profile of the polymer upon addition of mercuric bromide solution; as the concentration of the metal increased, the emission of the polymer decreased. Similar trends of emission quenching of the polymer were also observed with the other metals (Figures S6–S8 in the Supporting Information document) but to different extents.

Figure 7A displays Stern–Volmer plots for the relative change in the monomer emission of the polymer versus the increase in the concentration of the metal ions. The observed linear trends for the quenching of the fluorescence by the metal ions demonstrate that the strongest effects (Table 3) are for aluminum (K_{SV} = 152 M^{-1}) and mercury (K_{SV} = 143 M^{-1}) ions versus weaker effects for lead (K_{SV} = 32 M^{-1}) and thallium (K_{SV} = 19 M^{-1}) ions, whereas sodium, potassium, and calcium ions exhibit insignificant effects on the emission of Azo-Py.[36] Similar linear trends (Figure 7B) are also attainable for Benesi–Hildebrand plots, where the reciprocal of the

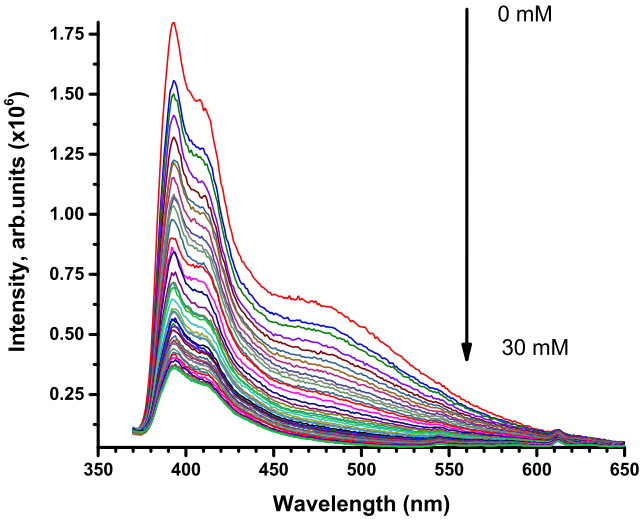

Figure 6. Emission spectra of Azo-Py (1.0 mg/mL) with successive additions of mercuric bromide (0.1 M) in acetonitrile.

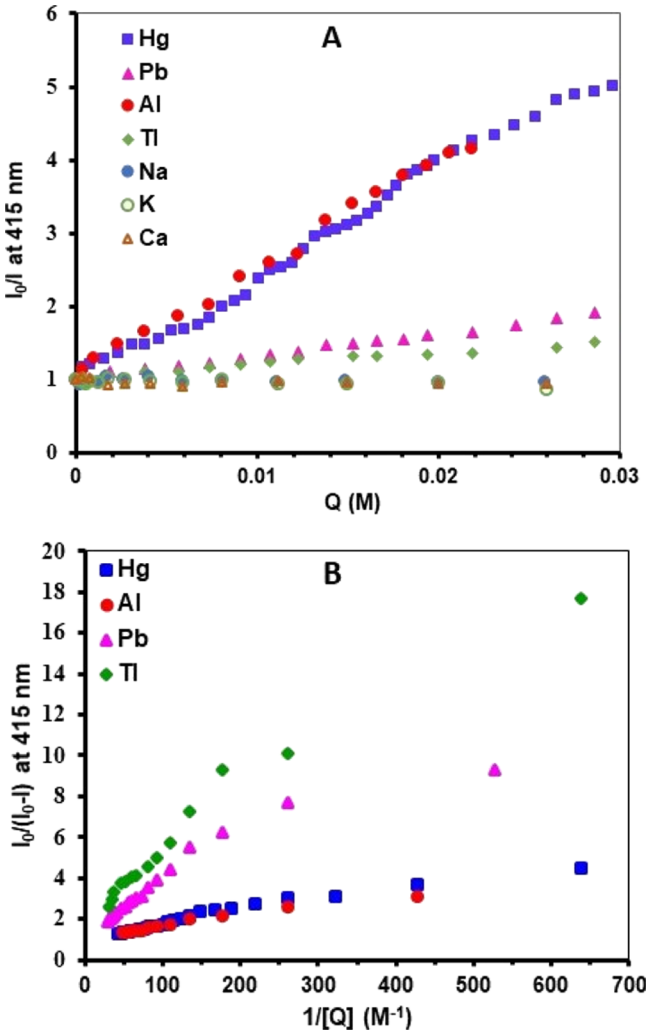

Figure 7. Stern–Volmer (A) and Benesi–Hildebrand (B) plots for the change in the emission (λ_{emi} = 415 nm) of Azo-Py upon titrating with the different metal ions.

change in the fluorescence intensity of the polymer is plotted versus the reciprocal of the metal concentrations. The linear

DOI: 10.1021/acsomega.8b01920
ACS Omega 2018, 3, 15510–15518

Table 3. Stern–Volmer (K_{SV}) Constants and Binding Constants (K_S) of Azo-Py with Various Metal Cations

metal cation	K_{SV} (M^{-1})	K_S (M^{-1})
Al^{3+}	152	376
Hg^{2+}	143	183
Pb^{2+}	31.9	120
Tl^{+}	19.1	112

fitting of these plots has provided the binding constants (Table 3) of the polymer to the metal ions, assuming a 1:1 binding ratio between the metal ion and each pyrene unit in the polymer. The obtained values indicated that interaction of aluminum (K_S = 376 M^{-1}) and mercury (K_S = 183 M^{-1}) ions with the polymer is stronger than that of lead (K_S = 121 M^{-1}) and thallium (K_S = 112 M^{-1}) ions, similar to conclusions based upon Stern–Volmer plots. We attribute this strong interaction and quenching effect of aluminum ions to their strong electrostatic attraction to the polymer (through azo-metal binding) because of the high concentration of charge, whereas for mercury ions it is due to the heavy atom effect resulting from spin–orbit coupling associated with cation-π coordination that disrupts excimer formation, consistent with the fluorescence spectral profile change, and quenches both the monomer and excimer fluorescence bands to different extents. Meanwhile, the low quenching effect of lead and thallium ions could be due to the hydration effect of the metal, which decreases the electrostatic metal-π binding.[50,51] Unlike Hg(II), these ions include valence electrons in the 6th shell, which could adversely impact the cation-π coordination via an electrostatic repulsive component. Finally, the hard ions of sodium, potassium, and calcium have very low affinity to both nitrogen atoms (azo group) and π-conjugated surfaces.

4. CONCLUSIONS

In conclusion, a new azo-functionalized porous organic polymer, Azo-Py, was synthesized by incorporating a highly conjugated pyrene core into the polymer framework. The influence of the pyrene moiety in the solid-state packing of the polymer is evident by the formation of nanofibers that are assembled by strong π–π stacking interactions manifest by excimer bands in the fluorescence spectra. Azo-Py displays high porosity with a surface area of 1259 m^2 g^{-1} and high microporosity as a result of the rigid pyrene core. These characteristics induce high CO_2 uptakes of 4.79 mmol g^{-1} (273 K) and 2.89 mmol g^{-1} (298 K) at 1 bar along with binding affinities conducive for easy regeneration, Q_{st} = 27.5 kJ mol^{-1}. Furthermore, Azo-Py because of its highly conjugated electron density has the ability to sense the electropositive heavy metal cations more selectively than harder cations. The ionic charge, atomic weight, and binding constant of the metal cation play a role in determining the extent of fluorescence quenching of the polymer's monomeric and excimeric pyrene-based emission bands.

■ ASSOCIATED CONTENT

Supporting Information

The Supporting Information is available free of charge on the ACS Publications website at DOI: 10.1021/acsomega.8b01920.

Porosity, gas uptake measurements, and emission spectra of Azo-Py with successive additions of metal ions in acetonitrile (PDF)

■ AUTHOR INFORMATION

Corresponding Authors

*E-mail: oelkadri@aus.edu. Phone +971 6 515-2787. Fax +971 6 515-2450 (O.M.E.-K.).

*E-mail: helkaderi@vcu.edu. Phone (804) 828-7505. Fax (804) 828-8599 (H.M.E.-K.).

ORCID

Mohammad H. Al-Sayah: 0000-0001-6321-0556

Mohammad A. Omary: 0000-0002-3247-3449

Hani M. El-Kaderi: 0000-0001-8770-1544

Notes

The authors declare no competing financial interest.

■ ACKNOWLEDGMENTS

T.-D.T. thanks Altria for graduate assistantship. O.M.E.-K. thanks the American University of Sharjah, grant# FRG17-R-12 and EFRG18-GER-CAS-67, for supporting this research project. M.A.O. acknowledges supporting aspects of his group's contributions by the Robert A. Welch Foundation (grant B-1542), National Science Foundation (CHE-1413641), and the Shenzhen Peacock Plan (no. 1208040050847074).

■ REFERENCES

(1) Zou, L.; Sun, Y.; Che, S.; Yang, X.; Wang, X.; Bosch, M.; Wang, Q.; Li, H.; Smith, M.; Yuan, S.; Perry, Z.; Zhou, H.-C. Porous Organic Polymers for Post-Combustion Carbon Capture. *Adv. Mater.* **2017**, *29*, 1700229.

(2) Arab, P.; Verlander, A.; El-Kaderi, H. M. Synthesis of a Highly Porous Bis(imino)pyridine-Linked Polymer and Its Postsynthetic Modification with Inorganic Fluorinated Ions for Selective CO_2 Capture. *J. Phys. Chem. C* **2015**, *119*, 8174–8182.

(3) Ben, T.; Pei, C.; Zhang, D.; Xu, J.; Deng, F.; Jing, X.; Qiu, S. Gas storage in porous aromatic frameworks (PAFs). *Energy Environ. Sci.* **2011**, *4*, 3991–3999.

(4) Popp, N.; Homburg, T.; Stock, N.; Senker, J. Porous imine-based networks with protonated imine linkages for carbon dioxide separation from mixtures with nitrogen and methane. *J. Mater. Chem. A* **2015**, *3*, 18492–18504.

(5) Fang, Q.; Gu, S.; Zheng, J.; Zhuang, Z.; Qiu, S.; Yan, Y. 3D Microporous Base-Functionalized Covalent Organic Frameworks for Size-Selective Catalysis. *Angew. Chem., Int. Ed.* **2014**, *53*, 2878–2882.

(6) Lin, S.; Diercks, C. S.; Zhang, Y.-B.; Kornienko, N.; Nichols, E. M.; Zhao, Y.; Paris, A. R.; Kim, D.; Yang, P.; Yaghi, O. M.; Chang, C. J. Covalent organic frameworks comprising cobalt porphyrins for catalytic CO_2 reduction in water. *Science* **2015**, *349*, 1208–1213.

(7) Ding, S.-Y.; Gao, J.; Wang, Q.; Zhang, Y.; Song, W.-G.; Su, C.-Y.; Wang, W. Construction of Covalent Organic Framework for Catalysis: Pd/COF-LZU1 in Suzuki-Miyaura Coupling Reaction. *J. Am. Chem. Soc.* **2011**, *133*, 19816–19822.

(8) Huang, Y.-B.; Wang, Q.; Liang, J.; Wang, X.; Cao, R. Soluble Metal-Nanoparticle-Decorated Porous Coordination Polymers for the Homogenization of Heterogeneous Catalysis. *J. Am. Chem. Soc.* **2016**, *138*, 10104–10107.

(9) Sun, Q.; Dai, Z.; Liu, X.; Sheng, N.; Deng, F.; Meng, X.; Xiao, F.-S. Highly Efficient Heterogeneous Hydroformylation over Rh-Metalated Porous Organic Polymers: Synergistic Effect of High Ligand Concentration and Flexible Framework. *J. Am. Chem. Soc.* **2015**, *137*, 5204–5209.

(10) Tong, W.; Li, W.-H.; He, Y.; Mo, Z.-Y.; Tang, H.-T.; Wang, H.-S.; Pan, Y.-M. Palladium-Metalated Porous Organic Polymers as Recyclable Catalysts for the Chemioselective Synthesis of Thiazoles from Thiobenzamides and Isonitriles. *Org. Lett.* **2018**, *20*, 2494–2498.

(11) Dalapati, S.; Jin, S.; Gao, J.; Xu, Y.; Nagai, A.; Jiang, D. An Azine-Linked Covalent Organic Framework. *J. Am. Chem. Soc.* **2013**, *135*, 17310–17313.

DOI: 10.1021/acsomega.8b01920
ACS Omega 2018, 3, 15510–15518

(12) Das, G.; Biswal, B. P.; Kandambeth, S.; Venkatesh, V.; Kaur, G.; Addicoat, M.; Heine, T.; Verma, S.; Banerjee, R. Chemical sensing in two dimensional porous covalent organic nanosheets. *Chem. Sci.* **2015**, *6*, 3931−3939.
(13) Li, Z.; Li, H.; Xia, H.; Ding, X.; Luo, X.; Liu, X.; Mu, Y. Triarylboron-Linked Conjugated Microporous Polymers: Sensing and Removal of Fluoride Ions. *Chem.—Eur. J.* **2015**, *21*, 17355−17362.
(14) Xiang, L.; Zhu, Y.; Gu, S.; Chen, D.; Fu, X.; Zhang, Y.; Yu, G.; Pan, C.; Hu, Y. A Luminescent Hypercrosslinked Conjugated Microporous Polymer for Efficient Removal and Detection of Mercury Ions. *Macromol. Rapid Commun.* **2015**, *36*, 1566−1571.
(15) Xiang, Z.; Cao, D. Synthesis of Luminescent Covalent-Organic Polymers for Detecting Nitroaromatic Explosives and Small Organic Molecules. *Macromol. Rapid Commun.* **2012**, *33*, 1184−1190.
(16) Sanders, S. N.; Kumarasamy, E.; Pun, A. B.; Trinh, M. T.; Choi, B.; Xia, J.; Taffet, E. J.; Low, J. Z.; Miller, J. R.; Roy, X.; Zhu, X.-Y.; Steigerwald, M. L.; Sfeir, M. Y.; Campos, L. M. Quantitative Intramolecular Singlet Fission in Bipentacenes. *J. Am. Chem. Soc.* **2015**, *137*, 8965−8972.
(17) Dogru, M.; Handloser, M.; Auras, F.; Kunz, T.; Medina, D.; Hartschuh, A.; Knochel, P.; Bein, T. A Photoconductive Thienothiophene-Based Covalent Organic Framework Showing Charge Transfer Towards Included Fullerene. *Angew. Chem., Int. Ed.* **2013**, *52*, 2920−2924.
(18) Raupach, M. R.; Marland, G.; Ciais, P.; Le Quere, C.; Canadell, J. G.; Klepper, G.; Field, C. B. Global and regional drivers of accelerating CO_2 emissions. *Proc. Natl. Acad. Sci. U.S.A.* **2007**, *104*, 10288−10293.
(19) Islamoglu, T.; Behera, S.; Kahveci, Z.; Tessema, T.-D.; Jena, P.; El-Kaderi, H. M. Enhanced Carbon Dioxide Capture from Landfill Gas Using Bifunctionalized Benzimidazole-Linked Polymers. *ACS Appl. Mater. Interfaces* **2016**, *8*, 14648−14655.
(20) Patel, H. A.; Je, S. H.; Park, J.; Chen, D. P.; Jung, Y.; Yavuz, C. T.; Coskun, A. Unprecedented high-temperature CO2 selectivity in N-2-phobic nanoporous covalent organic polymers. *Nat. Commun.* **2013**, *4*, 1357.
(21) Rabbani, M. G.; Sekizkardes, A. K.; El-Kadri, O. M.; Kaafarani, B. R.; El-Kaderi, H. M. Pyrene-directed growth of nanoporous benzimidazole-linked nanofibers and their application to selective CO_2 capture and separation. *J. Mater. Chem.* **2012**, *22*, 25409−25417.
(22) Nagaraja, C. M.; Haldar, R.; Maji, T. K.; Rao, C. N. R. Chiral Porous Metal Organic Frameworks of Co(II) and Ni(II): Synthesis, Structure, Magnetic Properties, and CO_2 Uptake. *Cryst. Growth Des.* **2012**, *12*, 975−981.
(23) Islamoglu, T.; Kim, T.; Kahveci, Z.; El-Kadri, O. M.; El-Kaderi, H. M. Systematic Postsynthetic Modification of Nanoporous Organic Frameworks for Enhanced CO_2 Capture from Flue Gas and Landfill Gas. *J. Phys. Chem. C* **2016**, *120*, 2592−2599.
(24) İslamoğlu, T.; Rabbani, M. G.; El-Kaderi, H. M. Impact of post-synthesis modification of nanoporous organic frameworks on small gas uptake and selective CO_2 capture. *J. Mater. Chem. A* **2013**, *1*, 10259−10266.
(25) Biswal, B. P.; Chandra, S.; Kandambeth, S.; Lukose, B.; Heine, T.; Banerjee, R. Mechanochemical Synthesis of Chemically Stable Isoreticular Covalent Organic Frameworks. *J. Am. Chem. Soc.* **2013**, *135*, 5328−5331.
(26) Gao, X.; Zou, X.; Ma, H.; Meng, S.; Zhu, G. Highly Selective and Permeable Porous Organic Framework Membrane for CO_2 Capture. *Adv. Mater.* **2014**, *26*, 3644−3648.
(27) Lu, W.; Sculley, J. P.; Yuan, D.; Krishna, R.; Wei, Z.; Zhou, H.-C. Polyamine-Tethered Porous Polymer Networks for Carbon Dioxide Capture from Flue Gas. *Angew. Chem., Int. Ed.* **2012**, *51*, 7480−7484.
(28) Buyukcakir, O.; Je, S. H.; Park, J.; Patel, H. A.; Jung, Y.; Yavuz, C. T.; Coskun, A. Systematic Investigation of the Effect of Polymerization Routes on the Gas-Sorption Properties of Nanoporous Azobenzene Polymers. *Chem.—Eur. J.* **2015**, *21*, 15320−15327.
(29) Patel, H. A.; Je, S. H.; Park, J.; Jung, Y.; Coskun, A.; Yavuz, C. T. Directing the Structural Features of N2-Phobic Nanoporous Covalent Organic Polymers for CO2 Capture and Separation. *Chem.—Eur. J.* **2014**, *20*, 772−780.
(30) Arab, P.; Rabbani, M. G.; Sekizkardes, A. K.; İslamoğlu, T.; El-Kaderi, H. M. Copper(I)-Catalyzed Synthesis of Nanoporous Azo-Linked Polymers: Impact of Textural Properties on Gas Storage and Selective Carbon Dioxide Capture. *Chem. Mater.* **2014**, *26*, 1385−1392.
(31) Wu, X.; Cobbina, S. J.; Mao, G.; Xu, H.; Zhang, Z.; Yang, L. A review of toxicity and mechanisms of individual and mixtures of heavy metals in the environment. *Environ. Sci. Pollut. Res.* **2016**, *23*, 8244−8259.
(32) Masten, S. J.; Davies, S. H.; McElmurry, S. P. Flint Water Crisis: What Happened and Why? *J.—Am. Water Works Assoc.* **2016**, *108*, 22−34.
(33) Upadhyay, P. K.; Marpu, S. B.; Benton, E. N.; Williams, C. L.; Telang, A.; Omary, M. A. A Phosphorescent Trinuclear Gold(I) Pyrazolate Chemosensor for Silver Ion Detection and Remediation in Aqueous Media. *Anal. Chem.* **2018**, *90*, 4999−5006.
(34) Bandyopadhyay, S.; Pallavi, P.; Anil, A. G.; Patra, A. Fabrication of porous organic polymers in the form of powder, soluble in organic solvents and nanoparticles: a unique platform for gas adsorption and efficient chemosensing. *Polym. Chem.* **2015**, *6*, 3775−3780.
(35) Kreno, L. E.; Leong, K.; Farha, O. K.; Allendorf, M.; Van Duyne, R. P.; Hupp, J. T. Metal-Organic Framework Materials as Chemical Sensors. *Chem. Rev.* **2012**, *112*, 1105−1125.
(36) Gupta, S. K.; Kaleeswaran, D.; Nandi, S.; Vaidhyanathan, R.; Murugavel, R. Bulky Isopropyl Group Loaded Tetraaryl Pyrene Based Azo-Linked Covalent Organic Polymer for Nitroaromatics Sensing and CO2 Adsorption. *ACS Omega* **2017**, *2*, 3572−3582.
(37) Yuan, Y.; Ren, H.; Sun, F.; Jing, X.; Cai, K.; Zhao, X.; Wang, Y.; Wei, Y.; Zhu, G. Sensitive detection of hazardous explosives via highly fluorescent crystalline porous aromatic frameworks. *J. Mater. Chem.* **2012**, *22*, 24558−24562.
(38) Räupke, A.; Palma-Cando, A.; Shkura, E.; Teckhausen, P.; Polywka, A.; Görrn, P.; Scherf, U.; Riedl, T. Highly sensitive gas-phase explosive detection by luminescent microporous polymer networks. *Sci. Rep.* **2016**, *6*, 29118.
(39) Zhang, C.; Jiao, N. Copper-Catalyzed Aerobic Oxidative Dehydrogenative Coupling of Anilines Leading to Aromatic Azo Compounds using Dioxygen as an Oxidant. *Angew. Chem., Int. Ed.* **2010**, *49*, 6174−6177.
(40) Jin, S.; Sakurai, T.; Kowalczyk, T.; Dalapati, S.; Xu, F.; Wei, H.; Chen, X.; Gao, J.; Seki, S.; Irle, S.; Jiang, D. Two-Dimensional Tetrathiafulvalene Covalent Organic Frameworks: Towards Latticed Conductive Organic Salts. *Chem.—Eur. J.* **2014**, *20*, 14608−14613.
(41) Sekizkardes, A. K.; İslamoğlu, T.; Kahveci, Z.; El-Kaderi, H. M. Application of pyrene-derived benzimidazole-linked polymers to CO_2 separation under pressure and vacuum swing adsorption settings. *J. Mater. Chem. A* **2014**, *2*, 12492−12500.
(42) Thommes, M.; Kaneko, K.; Neimark, A. V.; Olivier, J. P.; Rodriguez-Reinoso, F.; Rouquerol, J.; Sing, K. S. W. Physisorption of gases, with special reference to the evaluation of surface area and pore size distribution (IUPAC Technical Report). *Pure Appl. Chem.* **2015**, *87*, 1051−1069.
(43) Zhang, X.; Lu, J.; Zhang, J. Porosity Enhancement of Carbazolic Porous Organic Frameworks Using Dendritic Building Blocks for Gas Storage and Separation. *Chem. Mater.* **2014**, *26*, 4023−4029.
(44) Lu, J.; Zhang, J. Facile synthesis of azo-linked porous organic frameworks via reductive homocoupling for selective CO_2 capture. *J. Mater. Chem. A* **2014**, *2*, 13831−13834.
(45) Rabbani, M. G.; Reich, T. E.; Kassab, R. M.; Jackson, K. T.; El-Kaderi, H. M. High CO2 uptake and selectivity by triptycene-derived benzimidazole-linked polymers. *Chem. Commun.* **2012**, *48*, 1141−1143.
(46) Sekizkardes, A. K.; Altarawneh, S.; Kahveci, Z.; İslamoğlu, T.; El-Kaderi, H. M. Highly Selective CO_2 Capture by Triazine-Based

DOI: 10.1021/acsomega.8b01920
ACS Omega 2018, 3, 15510−15518

Benzimidazole-Linked Polymers. *Macromolecules* **2014**, *47*, 8328−8334.
(47) Saleh, M.; Baek, S. B.; Lee, H. M.; Kim, K. S. Triazine-Based Microporous Polymers for Selective Adsorption of CO_2. *J. Phys. Chem. C* **2015**, *119*, 5395−5402.
(48) Lee, J. H.; Lee, H. J.; Lim, S. Y.; Kim, B. G.; Choi, J. W. Combined CO_2-philicity and Ordered Mesoporosity for Highly Selective CO_2 Capture at High Temperatures. *J. Am. Chem. Soc.* **2015**, *137*, 7210−7216.
(49) Beyazkilic, P.; Yildirim, A.; Bayindir, M. Formation of pyrene excimers in mesoporous ormosil thin films for visual detection of nitro-explosives. *ACS Appl. Mater. Interfaces* **2014**, *6*, 4997−5004.
(50) Dougherty, D. A. The Cation-π Interaction. *Acc. Chem. Res.* **2013**, *46*, 885−893.
(51) Mahadevi, A. S.; Sastry, G. N. Cation − π Interaction : Its Role and Relevance in Chemistry , Biology , and Material Science. *Chem. Rev.* **2013**, *113*, 2100−2138.

DOI: 10.1021/acsomega.8b01920
ACS Omega 2018, 3, 15510−15518